Journal of Catalysis 320 (2014) 198–207

Contents lists available at ScienceDirect

Journal of Catalysis

journal homepage: www.elsevier.com/locate/jcat

Investigation of the reaction kinetics of isolated Lewis acid sites in Beta zeolites for the Meerwein–Ponndorf–Verley reduction of methyl levulinate to γ-valerolactone

Helen Y. Luo, Daniel F. Consoli, William R. Gunther, Yuriy Román-Leshkov *

Department of Chemical Engineering, Massachusetts Institute of Technology, Cambridge, MA 02139, United States

ARTICLE INFO

Article history:
Received 29 August 2014
Accepted 19 October 2014

Keywords:
Liquid-phase transfer hydrogenation
γ-Valerolactone
Lewis acids
Zeolites
Reaction kinetics

ABSTRACT

We investigate the reaction kinetics of the Meerwein–Ponndorf–Verley (MPV) reduction of methyl levulinate (ML) to 4-hydroxypentanoates and subsequent lactonization to γ-valerolactone (GVL) catalyzed by Lewis acid zeolites. Reaction kinetics studies show a first-order dependence on ML and 2-butanol, confirm that the hydride shift is the rate-limiting step, and support a dual-binding mechanism on a single Lewis acid site. All catalysts generate GVL with selectivities >97%, with Hf-Beta exhibiting the highest activity in the temperature range of 393–453 K. Sn-, Zr-, and Hf-Beta show apparent activation energies of ca. 52 kJ mol^{-1}, which is significantly lower than that of Ti-Beta (69 kJ mol^{-1}). Secondary alcohols consistently exhibit higher reaction rates than primary alcohols with lower apparent activation energies. Increasing polarity of the hydrogen donor leads to a decrease in reaction rates. The experimental data are used to build a kinetic model for the MPV reaction in a tubular packed-bed reactor.

1. Introduction

Biomass conversion to sustainable chemicals and fuels requires the development of efficient catalytic processes capable of converting highly complex and oxygenated precursors to platform molecules. Ideally, selective deoxygenation and hydrogenation must occur under mild conditions while simultaneously minimizing unit operations. Transfer hydrogenations are versatile reactions that avoid the use of high pressures of molecular hydrogen by using molecules capable of donating hydrogen atoms in the liquid phase [1–5]. In particular, the Meerwein–Ponndorf–Verley (MPV) reaction, wherein an alcohol donates a hydride to an aldehyde or ketone, has shown promising results in several biomass-relevant reaction schemes. Examples include the conversion of the following: crotonaldehyde to crotyl alcohol [6]; 5-(hydroxymethyl) furfural to 2,5-bis(ethoxymethyl)furan [7]; levulinates to γ-valerolactone [8,9]; and intramolecular hydride transfers in hexoses, pentoses, and other sugars [10–19].

Traditionally, homogenous Lewis acids catalyze the MPV reaction as shown for aluminum alkoxides [20,21] in an isopropanol/ketone system, for lanthanide complexes in the reduction of aryl ketones [22], and more recently for actinide isopropoxides [23]. The reaction mechanism involves a cyclic six-membered transition state where the carbonyl and the alcohol are both coordinated to the same metal center. The reaction proceeds through a direct hydride shift where the hydrogen on the C-1 position of the alcohol is directly transferred to the carbonyl carbon of the ketone/aldehyde. To overcome the problems associated with using homogenous catalysts, such as expensive separations and moisture sensitivity, many heterogeneous catalysts have been studied for the MPV reaction. These include metal oxides [24,25], hydrotalcites [26,27], and zeolites [28–32]. In particular, zeolites containing Lewis acid centers have shown very high activity and selectivity under mild reaction conditions [33–36]. Lewis acidic metal centers tetravalently incorporated into a silicate framework can coordinate with and polarize carbonyl functional groups [37,38]. It is proposed that these metal centers coordinate the ketone and alcohol to form the same six-membered transition state as that formed with homogenous MPV catalysts. Various Lewis acid zeolites are capable of catalyzing the MPV reaction including Al-, Ti-, Sn-, and Zr-containing zeolites.

Recently, we reported on the one-pot conversion of xylose-derived furfural into γ-valerolactone (GVL) using the combined action of zeolites featuring Lewis and Brønsted acid sites [8]. GVL is a versatile platform molecule that has the functionality and reactivity to be upgraded to fuel additives, fuels, and commodity chemicals [39–43]. GVL is stable, non-toxic and has shown promise as an effective solvent for sugar production by breaking down

* Corresponding author.
E-mail address: yroman@mit.edu (Y. Román-Leshkov).

http://dx.doi.org/10.1016/j.jcat.2014.10.010
0021-9517/

lignocellulosic biomass [44]. In our domino-like reaction sequence, furfural was reduced to furfuryl alcohol (FA) via an MPV reaction with 2-butanol catalyzed by a Lewis acid; next, FA was converted to levulinic acid (LA) through a hydrolytic ring opening catalyzed by a Brønsted acid; finally, LA was reduced via a second MPV step to 4-hydroxypentanoate (4HP), which underwent a spontaneous lactonization to form GVL and water. GVL selectivity values always exceeded 94%, but it was observed that Ti-, Sn-, and Zr-Beta catalysts featured drastically different turnover rates for the second MPV step, with Zr-Beta having the highest activity. Assary et al. showed with computational techniques that stronger Lewis acids better stabilize the six-membered transition state for the rate-limiting hydride shift step [45]. Indeed, changing the identity of the framework heteroatom can alter the Lewis acid character of the zeolite; however, Lewis acidity is also highly dependent on the nature of the solvent and reacting molecules. A difficult challenge exists in correctly predicting which catalyst will be optimal for a specific substrate/solvent combination. For example, Boronat et al. showed that while Sn-Beta is more active for the reduction of cyclohexanone in 2-butanol, Zr-Beta is more active for the reduction of benzaldehyde in 2-butanol under identical reaction conditions [46]. The nature of the hydrogen donor also had a dramatic impact on the reaction rates. As such, establishing a robust kinetic framework that describes the governing parameters of the ML to GVL transformation over a wide range of conditions is of great relevance to understand, and ultimately predict, the performance of Lewis acid zeolites in transfer hydrogenation reactions.

In this work, we present an experimental study aimed at extracting relevant kinetic parameters that describe the catalytic performance of Lewis acid catalysts during the reduction of ML to form GVL. We propose a set of elementary steps, derive a rate expression for the overall reaction, and perform reactivity measurements to confirm reaction orders and identify the rate-limiting step in the mechanism. We quantitatively compare the kinetic parameters of Ti-, Sn-, Zr-, and Hf-Beta catalysts over a wide range of temperatures and find that Hf-Beta has the highest activity of all catalysts. We also study the effect of varying the hydrogen donor by determining the kinetic parameters when using primary and secondary alcohols with varying carbon chain lengths.

2. Experimental methods

2.1. Catalyst synthesis

Lewis acid zeolites with the Beta topology were synthesized in fluoride media following the procedure outlined by Corma et al. [47], using different heteroatom metal precursors. For example, Hf-Beta was prepared as follows: 27.16 g of tetraethylammonium hydroxide (Sigma–Aldrich, 35% (w/w) in water) and 23.97 g of tetraethylorthosilicate (Sigma–Aldrich, $\geqslant$99% (w/w)) were added to an open Teflon jar. The mixture was magnetically stirred at room temperature for 90 min. An additional 15 ml of deionized water was added and the mixture was cooled in an ice bath. Then, 0.37 g of hafnium(IV) chloride (Sigma–Aldrich, 98% (w/w)) was dissolved in 2 ml of ethanol, and this solution was added dropwise to the mixture while stirring on ice. The solution was left uncovered while stirring to complete the hydrolysis of TEOS, evaporate the ethanol, and reach approximately 2 g of water above the target water content. Then, 2.62 g of hydrofluoric acid (Sigma–Aldrich, 48% (w/w) in water) was added dropwise and the mixture was homogenized using a PTFE spatula, resulting in a thick paste. Next, 0.36 g of previously-made Hf-Beta was sonicated in 2 ml deionized water and added into the mixture as seeds. The mixture was homogenized and allowed to evaporate to a final weight of 33.96 g. The final molar composition of the gel was 1 SiO_2/0.01 $HfCl_4$/0.56 TEAOH/0.56 HF/7.5 H_2O. The thick paste was transferred to a Teflon-lined stainless steel autoclave and heated to 413 K in a static oven for 20–40 days. The solids were recovered by filtration, washed extensively with water and ethanol, and dried at 373 K overnight. The solids were calcined at 923 K for 10 h with a 1 K/min ramp and 1 h stops at 423 K and 623 K at a flow rate of 300 ml min^{-1} of dry air (Airgas, ultra zero grade) to remove the organic content in pores of the crystalline material. After calcination, the solid yield was 80–90%. The other metal precursors used were as follows: tin(II) chloride dihydrate (Sigma–Aldrich, 99.99% (w/w)), zirconium(IV) oxychloride octahydrate (Sigma–Aldrich, 99.5% (w/w)), and titanium(IV) isopropoxide (Sigma Aldrich, 99.999% (w/w)). All the catalysts were synthesized to achieve a silicon/metal ratio of ca. 100.

2.2. Catalyst characterization

The crystal structures of Beta zeolite catalysts were determined from powder X-ray diffraction (PXRD) patterns collected using a Bruker D8 diffractometer using Cu Kα radiation (40 kV, 40 mA). Nitrogen adsorption and desorption isotherms were measured on a Quantachrome Autosorb iQ apparatus at liquid nitrogen temperature (77 K). Prior to the adsorption analysis, all samples were pelleted and degassed under vacuum for 12 h at 623 K. Micropore N_2 uptake was recorded at $P/P_0 = 0.01$, and total pore volume was recorded at $P/P_0 = 0.95$. Ultraviolet–visible (UV–vis) spectra were recorded using a Cary 5000 (Varian) instrument equipped with a Praying Mantis diffuse-reflectance accessory (Harrick Scientific Products) on calcined samples using a barium sulfate blank. Reflectance measurements were converted to absorbance using the Kubelka–Munk function. Elemental analysis was performed with a CCD-based inductively coupled plasma (ICP) atomic emission spectrometer (Activa-S, HORIBA Scientific). Samples were dissolved in 48% HF and diluted into 3% HNO_3 before analysis. A 5-point calibration curve was built using the following ICP standards: 1000 ppm Zr in 3% HNO_3/trace HF, 1000 ppm Sn in 10% HCl, 1000 ppm Ti in 2% HNO_3/trace HF, 1000 ppm Hf in 5% HNO_3/trace HF (all TraceCERT®) on the following spectral lines: 327.305 nm Zr line, 189.989 nm Sn line, 339.978 nm Hf line, 336.121 nm Ti line.

Fourier transform infrared (FT-IR) spectra were collected with a Bruker Vertex 70 spectrophotometer equipped with an Hg–Cd–Te (MCT) detector. Each spectrum was recorded by averaging 128 scans at 2 cm^{-1} resolution in the 4000–400 cm^{-1} range. Zeolite-beta catalysts were pressed into self-supporting wafers (8–10 mg cm^{-2}) that were sealed within a high temperature cell (Harrick Scientific) with ZnSe windows. Zeolite wafers were calcined in flowing air (Airgas, zero grade, 25 ml min^{-1}) at 773 K for 8 h, evacuated at 573 K for 3 h (<0.01 Pa, dynamic vacuum, Edwards' T-Station 75 Turbopump), and cooled to 298 K in vacuum. A reference spectrum was acquired before dosing with excess CD_3CN (Sigma Aldrich, 99.8% (atom D)) vapor under static vacuum. Once dynamic vacuum was re-established, the difference spectrum was acquired.

2.3. Kinetic studies of MPV reduction of levulinates

Flow reactions were conducted in a 0.46 cm I.D. tubular stainless steel reactor mounted inside a 30 cm long aluminum block within an insulated single-zone furnace (Applied Test Systems Series 3210, 850W/115 V). The catalyst was pelleted and sieved to obtain 75–150 μm particles. The catalyst particles were then diluted into 5 times their weight in inert α-aluminum oxide (Sigma Aldrich, >99% (w/w)) with the same particle size range, creating a bed approximately 2.5 cm long. The bed was loaded between glass wool plugs and supported by additional α-aluminum oxide. The reaction temperature was monitored by a K-type thermocouple (Omega, inconel) placed inside the bed and a PID temperature controller

(Cole-Parmer, Digi-Sense Advanced Temperature Controller Series 89000). Prior to reaction, the packed bed was dried under flowing N_2 gas (Airgas, grade 5, 300 ml min^{-1}) at 423 K for 2 h. Liquid-phase reactants were introduced with a Waters 515 HPLC pump, and the entire system was pressurized under 15–20 bar of N_2 using a back-pressure regulator (Swagelok). The effluent was collected in a high-pressure separator (Jerguson Gage and Valve Co., Series R20) at room temperature.

For sample quantification, a known amount of 1,3,5-tri-tert-butylbenzene (Sigma Aldrich, 97% (w/w)) in the same solvent as the effluent was added as an external standard. Liquid samples were analyzed by gas chromatography (Agilent 6890N) equipped with a methoxy-siloxane capillary column (HP-1, 30 m × 0.25 mm × 0.25 μm) connected to a flame ionization detector. All mass balances exceeded 97% for all experiments. The conversions are determined based on initial and final ML concentrations, and the reaction rates are calculated based on GVL yield. In the runs where methyl levulinate is used as a solvent, the rates and conversions are based on the alcohol reactant. Conversion is defined as follows:

$$X = 1 - \frac{C_{ML}}{C_{ML,0}} \quad (1)$$

$$X_{ML,solvent} = 1 - \frac{C_{X\text{-}OH}}{C_{X\text{-}OH,0}} \quad (2)$$

Yield is defined as follows:

$$Y = \frac{C_{GVL}}{C_{ML,0}} \quad (3)$$

$$Y_{ML,solvent} = \frac{C_{X=O}}{C_{X\text{-}OH,0}} \quad (4)$$

where X is the conversion, Y is the yield, C_i is the molar concentration (mol dm^{-3}) of species i recovered in a given reactor sample, and $C_{i,0}$ is the initial concentration of reactant fed at a constant volumetric flow rate.

Kinetic studies were conducted in a differential reactor bed in which levulinate conversion was controlled to be <10%. For some runs, a small amount of ethyl, propyl, or butyl levulinate (XL) production was observed when using ML as the reactant, but total ML conversion was always kept below 10%. The other levulinates undergo an identical reduction to ML and generate variants of 4HP, which subsequently lactonize to GVL; consequently, they are treated as equivalent to ML in the overall reactant pool and do not affect GVL selectivity negatively. Selectivity is defined as follows:

$$S_{GVL} = \frac{C_{GVL}}{C_{ML,0} - C_{ML} - C_{XL}} \quad (5)$$

Volumetric flow rates for the activation energy studies and order studies ranged from 0.5 to 2.5 ml min^{-1} corresponding to space velocities ranging from 0.1 to 10^3 (mol reactant)(mol metal s)$^{-1}$. The concentration of reactant was kept at 0.02 mol dm^{-3} for activation energy studies and in the range of 0.0075–0.03 mol dm^{-3} for reaction order studies. Activation energy experiments were performed in a temperature range of 393–453 K, and all other studies were performed at 423 K. Reactants and solvents used were as follows: 2-butanol, 2-propanol, 1-butanol, 1-propanol (Sigma Aldrich, ⩾99.5% (w/w) anhydrous); ethanol (Koptec, 99.5% (v/v) anhydrous); 2-propanol-d_8 (Sigma Aldrich, 99.5% (atom D), anhydrous); methyl levulinate (Sigma Aldrich, ⩾98% (w/w)). Solvents were dried with activated 4 Å molecular sieves (Sigma Aldrich, 4–8 mesh beads) prior to use.

3. Results and discussion

3.1. Synthesis and characterization of Ti-, Sn-, Zr-, and Hf-containing Beta zeolites

Characterization data of all Beta catalysts are given in Table 1. X-ray diffraction patterns (Fig. S1, Supporting Information) of Ti-, Sn-, Zr-, and Hf-Beta were consistent with the BEA topology. The asymmetry of the peak in the range of 2θ = 7–9° in the Hf-Beta and Zr-Beta powder patterns indicates an increase in the relative proportion of the polymorph B in the crystal structure, an effect previously reported for Zr-Beta by Zhu et al. [32]. No peaks due to metal oxide or other crystalline impurities were detected. The micropore volumes of all catalysts, calculated from the nitrogen adsorption isotherms at 77 K (Fig. S3, Supporting Information), were consistent with the Beta topology measuring ca. 0.20 $cm^3\ g^{-1}$ at P/P_0 = 0.01. The slight variations in total pore volume and external surface area indicate slight differences in crystal size and morphology between the samples. Elemental analysis by ICP-AES shows Si/M ratios in the range of 108–121, close to the theoretical value of 100 used in the synthesis gels. Synthesizing these zeolites in fluoride media has been shown to produce defect-free frameworks, which translate to pore structures with high hydrophobicity [10].

The presence of isolated Lewis acidic M^{4+} centers incorporated in the framework of the zeolites was demonstrated qualitatively by diffuse-reflectance UV–vis spectroscopy, which shows a single peak at ~200 nm for each catalyst (Fig. S2, Supporting Information). The absence of peaks or shoulders in the 230–250 nm range indicates a lack of detectable MO_x species. Extraframework MO_x species can catalyze the MPV reaction, but do so at rates that are negligible with respect to the rates observed for framework species. IR spectra of Ti- and Sn-Beta collected after saturation with CD_3CN and subsequent evacuation at 298 K (Fig. S4, Supporting Information) shows bands at ~2308–2316 cm^{-1} consistent with C≡N stretching vibrations for CD_3CN bound to Lewis acidic centers, and at ~2276 cm^{-1} for CD_3CN bound to silanol groups [48,49]. These spectra indicate the presence of Lewis acid centers as well as Brønsted acidic hydroxyl groups in the Beta catalysts.

3.2. Proposed mechanism for MPV reaction over metal sites and reaction order studies

The reduction of ML to 4HP and subsequent intramolecular lactonization over Hf-Beta in excess 2-butanol (BuOH) at 423 K yields only one major product, GVL, for ML conversions ranging from 1% to 100%. The intermediate 4HP could not be detected, which indicates that the intramolecular ring closing is very fast at the reaction conditions investigated. Abdelrahman et al. showed that in the presence of Brønsted acidity and temperatures above 323 K, lactonization rates are high, leading to high GVL selectivity and the absence of detectable 4HP intermediates [50]. A small amount of butyl levulinate (BL) is observed (<5%), indicating a concurrent acid-catalyzed esterification of ML with BuOH. This side reaction does not alter the reaction pathway since BL can be converted to GVL along the exact same mechanism as that for ML.

Table 1
Catalyst site and structural characterization.

Catalyst	Si/M	$V_{ads}(N_2)$ ($cm^3\ g^{-1}$) micropore[a]	$V_{ads}(N_2)$ ($cm^3\ g^{-1}$) total[b]
Ti-Beta	108	0.20	0.33
Hf-Beta	121	0.20	0.30
Zr-Beta	111	0.20	0.29
Sn-Beta	108	0.20	0.34

[a] N_2 volume at end of micropore filling transition (77 K) at P/P_0 = 0.01.
[b] N_2 volume at P/P_0 = 0.95.

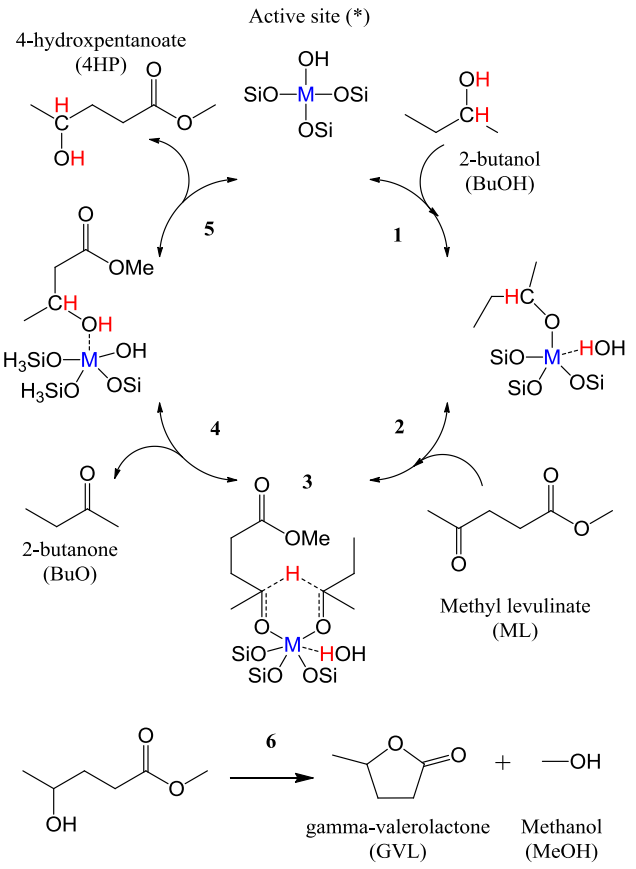

Scheme 1. Proposed catalytic cycle for the MPV reduction of methyl levulinate (ML) to 4-hydroxypentanoate (4HP) with 2-butanol (BuOH) over a partially hydrolyzed metal site in zeolite framework (*). BuOH adsorbs and deprotonates (1), ML then adsorbs (2) and converts to 4HP through a hydride shift in a six-membered transition state (3), 2-butanone (BuO) desorbs (4), 4HP receives a proton from the catalyst and desorbs (5), and 4HP undergoes spontaneous lactonization producing GVL and methanol (MeOH) (6).

A proposed catalytic cycle for the MPV reaction of ML with BuOH over a single catalytic center in Beta zeolite based on a set of elementary steps is shown in Scheme 1. The catalytic cycle is consistent with previously proposed mechanisms for the MPV reaction [46]. The active Lewis acid site is hypothesized to be a partially hydrolyzed "open site" where the metal is coordinated to three O—Si framework groups and one hydroxyl group [48]. The reaction proceeds in the following steps: adsorption and deprotonation of BuOH over the Lewis acid center (step 1); adsorption of ML (step 2) and hydride shift from deprotonated BuOH to ML through a six-membered cyclic transition state (step 3); desorption of 2-butanone (BuO) (step 4); and hydrogen transfer from the catalyst and desorption of 4HP (step 5). 4HP then undergoes a spontaneous intramolecular ring-closure and a Brønsted acid-catalyzed release of methanol (MeOH) to form GVL (step 6). Based on computational studies, the hydride shift is the slowest step in the mechanism and constitutes the rate-determining step. We further assume that all adsorption and desorption steps are in quasi-equilibrium, that all species in the reaction including small amounts of residual water (H_2O) can act as singly-bound inhibitors and that the intramolecular lactonization of 4HP is very fast and irreversible (Scheme A2, Appendix A). The fast lactonization step results in a product sink making the concentration of 4HP very small, and consequently, the reverse reaction of step 3 (i.e., 4HP back to ML) is negligible. A rate expression for the rate of GVL production normalized per catalytic site (mol (mol metal s)$^{-1}$) is given by Eq. (6).

$$r' = \frac{k_{f,H} K_{ML^*} K_{BuOH} C_{ML} C_{BuOH}}{D}$$

$$D = 1 + K_{ML}C_{ML} + K_{BuOH}C_{BuOH} + K_{GVL}C_{GVL} + K_{H_2O}C_{H_2O} + K_{4HP}C_{4HP} + K_{MeOH}C_{MeOH} + K_{BuO}C_{BuO} \quad (6)$$

In this equation, C_i terms are liquid-phase concentrations (mol dm^{-3}) for species i, and K_i are the equilibrium constants (dm^3 · mol^{-1}) relating liquid-phase species to species that are singly bound to the Lewis sites (Scheme A2). K_{ML^*} is the equilibrium constant relating free ML to ML bound specifically to sites that already have a bound BuOH molecule. $k_{f,H}$ is the forward rate constant (s^{-1}) for the hydride shift.

In excess of BuOH, we can assume BuOH* constitutes the majority of bound species on the acid sites. Therefore, the third term in the denominator dominates over the others, leading to the further simplified expression (Eq. (7)), which shows first-order dependence on ML concentration. The expression for the apparent rate constant is given in Eq. (8), and the expression for the apparent activation energy (E_a) consisting of the activation energy of the hydride shift and the enthalpy of adsorption of ML onto an already occupied site, is given in Eq. (9).

$$r' = (k_{f,H} K_{ML^*}) C_{ML} \quad (7)$$

$$k_{app,BuOH} = k_{f,H} K_{ML^*} \quad (8)$$

$$E_{a,app,BuOH} = E_{a,H} + \Delta H_{ads,ML^*} \quad (9)$$

Conversely, in excess ML, we can assume ML* constitutes the majority of bound species on the acid sites. Therefore, the second term in the denominator dominates over the others, leading to the further simplified expression (Eq. (10)), which shows first-order dependence on BuOH concentration. If we assume that K_{ML} is approximately equal to K_{ML^*}, then the apparent rate constant in excess ML is simplified to Eq. (11). This gives an expression for the apparent E_a (Eq. (12)), which consists of the activation energy of the hydride shift and the enthalpy of adsorption of 2-BuOH onto an unoccupied site.

$$r' = \left(\frac{k_{f,H} K_{ML^*} K_{BuOH}}{K_{ML}}\right) C_{BuOH} \quad (10)$$

$$k_{app,ML} = k_{f,H} K_{BuOH} \quad (11)$$

$$E_{a,app,ML} = E_{a,H} + \Delta H_{ads,BuOH} \quad (12)$$

The initial turnover frequencies were measured in terms of GVL production normalized by total metal content of zeolite, at an ML conversion <10%. As shown in Fig. 1, first-order dependencies of initial rates to ML concentration in solvent excess of BuOH and of BuOH concentration in solvent excess of ML are confirmed by slope values of the log rate vs. log initial concentration plots that approach unity. These first-order dependencies support our proposed mechanism where both reactant molecules are coordinated to a single catalytic center. These data are in agreement with several computational studies on the MPV reaction over Beta zeolites using density functional theory [45,46], as well as the established mechanism for MPV reaction on Al(III) isopropoxide [20].

3.3. Exclusion of mass transport limitations and confirmation of rate-determining step

Measured initial rates would also show an apparent first-order dependence on ML or BuOH concentration for a process limited by the diffusion of reactants to active sites located within the zeolite pores. To rule out intercrystalline heat and mass transport artifacts, the linear velocity in the reactor was varied while maintaining a constant space velocity at temperatures of 393, 423, and 453 K.

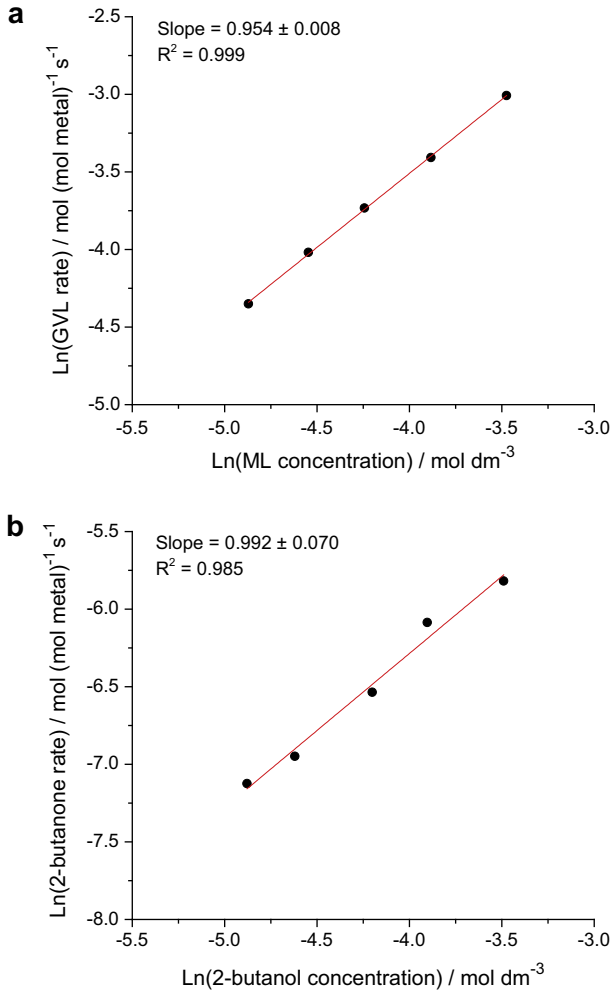

Fig. 1. Log–log plot of initial rates vs. methyl levulinate (ML) concentration in solvent excess of 2-butanol (BuOH) (a), and BuOH concentration in solvent excess of ML (b) for Hf-Beta catalyst. Rates are measured in moles of GVL produced per second normalized per total mole metal center in the catalyst. In excess ML, rates are measured in moles of 2-butanone produced per second normalized per total metal center in the catalyst. The standard error of regression is calculated assuming errors are normally distributed and the sum of square residuals is χ^2 distributed with $n-2$ degrees of freedom. All liquid-phase flow reactions were performed under differential conditions in a packed-bed reactor pressurized under nitrogen at 15 bar with a flow rate of 1.0 ml min^{-1}, at temperature 423 K, with feed concentrations of 0.0075–0.03 mol dm^{-3} reactant.

As shown in Fig. S5, the rate of GVL production remains constant (within experimental error) for all linear velocities at the full range of temperatures, indicating that no external mass transfer limitations exist at these conditions. Next, to ensure the absence of intracrystalline heat and mass transport artifacts, turn over frequencies for Hf-Beta zeolites with varying Si/M ratios were measured and compared. Initial rates were determined for Hf-Beta200 (Si/Hf ratio of 190, as confirmed by ICP-AES elemental analysis) and Hf-Beta300 (Si/Hf ratio of 336) under identical kinetic reaction conditions to those used for the original Hf-Beta catalyst at 393, 423, and 453 K. As shown in Fig. S6, the rates normalized per total metal site are constant for all temperatures tested, thus confirming that the reaction conditions used in this study satisfy the Koros–Nowak criterion and do not exhibit internal heat or mass transport limitations. All kinetic data were collected in the absence of significant catalyst deactivation, as confirmed by replicating initial runs in a series and obtaining identical activity values.

To support our hypothesis that the rate-limiting step of the reaction is the hydride shift, we measured the kinetic isotope effect (KIE) using 2-propanol-H_8 and 2-propanol-D_8 as the solvent. The $k_{app,H}/k_{app,D}$ ratio at 423 K was 2.01 ± 0.33 (Table S1, Supporting Information). This KIE value indicates that the elementary steps for adsorption and deprotonation do not limit rates of ML hydrogenation prior to the kinetically-relevant hydride shift. Incorporation of the deuteron in the C-4 position in the GVL product was confirmed by ^{1}H NMR (Fig. S7, Supporting Information). The same effect can be seen when performing the experiment in excess ML where the $k_{app,H}/k_{app,D}$ ratio at 423 K was 1.90 ± 0.10 (Table S1, Supporting Information). Previous studies on the MPV reduction catalyzed by homogenous aluminum(III) complexes have yielded experimental KIE values of 2.3 and 3.0 [20,51]. The exact nature of the vibrational mode of the bimolecular six-membered transition state is difficult to determine for heterogeneous catalytic sites even with density functional theory (DFT) given the need to use tight convergences for the force constants and appropriate dispersive interactions to locate the transition states. At the given temperatures, assuming the transition state oscillation is a combination of C—H bond scissoring (~1400 cm^{-1}) and C—H bond stretching (~2900 cm^{-1}), a theoretical KIE value between 1.9 and 3.6 is expected (see derivation in section A, Supporting Information). Given the absence of mass transfer limitations, our experimental KIE values imply that the bending vibrational mode is dominant in the transition state, possibly due to confinement in the narrow zeolite pores.

3.4. Temperature effects

Having established reaction orders and ruled out heat and mass transfer limitations, the apparent rate constant k_{app} and Arrhenius parameters were explicitly determined under differential reaction conditions in a temperature range of 393–453 K (Table 2). The apparent activation energy for the reaction over Hf-Beta catalyst in excess of BuOH is 52.5 ± 1.9 kJ mol^{-1} and the pre-exponential factor is 4.1 × 10^6 (mol dm^3)(mol metal s mol ML)$^{-1}$. This apparent activation energy agrees well with that found for levulinic acid hydrogenation in liquid water using Ru-based catalysts (48 kJ mol^{-1}) [50]. In addition, the experimental value matches closely with the apparent activation energy of 53.9 kJ mol^{-1} calculated by Assary et al. for ethyl levulinate in isopropanol solvent over Zr-Beta catalyst [45]. We would expect Hf and Zr sites to behave very similarly due to their comparable electronic properties and atomic sizes. The activation energy for the reaction over Hf-Beta catalyst in excess ML is 44.8 ± 1.4 kJ mol^{-1}, and the pre-exponential factor is 3.8 × 10^4 (mol dm^3)(mol metal s mol BuOH)$^{-1}$. The decrease in apparent activation energy is attributed to the stronger adsorption of ML on the metal site compared to the adsorption of BuOH on the metal site based on the simplified rate expressions (Eqs. (7) and (10)). This trend agrees with the theoretical difference in adsorption enthalpies of ML and BuOH of 14.2 kJ mol^{-1} calculated by Assary et al. [45]. In addition, the two order of magnitude difference in the pre-exponential factors when switching solvents leads to a large difference in the free energies of adsorption, which is reflected by an order of magnitude decrease in the apparent rate constant at 423 K. More specifically, k_{app} is 0.110 (mol dm^3) (mol metal s mol BuOH)$^{-1}$ when operating in excess ML compared to 1.33 (mol dm^3)(mol metal s mol ML)$^{-1}$ when operating in excess BuOH.

3.5. Comparison of Ti, Sn, Zr, Hf-Beta catalysts

The MPV reduction of ML has previously been shown to occur with high activity and selectivity over Sn- and Zr-Beta catalysts in batch reactions. Although previous studies in liquid-phase batch reactors report very low conversions for Ti-Beta (~1%), we now quantitate its turnover rate for the MPV reaction [8]. Our results

Table 2
Measured first-order rate constants, activation energies and pre-exponential factors for MPV reduction of methyl levulinate (ML) in hydrogen-donating solvent 2-butanol (BuOH) with various zeolite-beta catalysts. Rates are measured in moles of GVL produced per second normalized per total mole metal center in the catalyst. All liquid-phase flow reactions were performed in a packed-bed reactor pressurized under nitrogen at 20 bar with a flow rate range of 0.5–2.5 ml/min, with temperature range of 393–453 K.

Run	Catalyst	Feed (mol dm^{-3})	Solvent	Rate constant k_{app} at 423 K[a]	Apparent E_a (kJ mol^{-1})	Standard error[b] (kJ mol^{-1})	Pre-exponential factor A[c]	Standard multiplicative error[b,c]
1	Hf-Beta	0.02 ML	BuOH	1.33E+0	52.5	1.9	41.3	1.7
2	Hf-Beta	0.02 BuOH	ML	1.10E−1[d]	44.8	1.4	0.382[e]	1.5
3	Zr-Beta	0.02 ML	BuOH	6.84E−1	51.8	1.0	17.3	1.3
4	Sn-Beta	0.02 ML	BuOH	1.92E−1	51.7	2.1	5.1	1.8
5	Ti-Beta	0.02 ML	BuOH	5.26E−4	69.0	2.2	1.8	1.9

[a] Units: (mol dm^3)(mol metal s mol ML)$^{-1}$.
[b] Standard error of regression assuming errors are normally distributed, sum of square residuals is χ^2 distributed with $n-2$ degrees of freedom.
[c] Units: 10^5 (mol dm^3)(mol metal s mol ML)$^{-1}$.
[d] Units: (mol dm^3)(mol metal s mol BuOH)$^{-1}$.
[e] Units: 10^5 (mol dm^3)(mol metal s mol BuOH)$^{-1}$.

show that Hf-Beta converts ML to GVL in BuOH with high selectivity and with a rate constant (1.33 (mol dm^3)(mol metal s mol ML)$^{-1}$) that is twice as large than that of Zr-Beta (0.684 (mol dm^3)(mol metal s mol ML)$^{-1}$), and seven times larger than that of Sn-Beta (0.192 (mol dm^3)(mol metal s mol ML)$^{-1}$) at 423 K (Table 2). The marked differences in initial rates between the catalysts that arise in spite of the similar apparent activation energy values of 52.5 ± 1.9, 51.8 ± 1.0, and 51.7 ± 2.1 kJ mol^{-1} for Hf-, Zr-, and Sn-Beta, respectively (Table 2), highlight the need to find the optimal Lewis acid catalyst for each reaction system. The activation energies and activities depend on the Lewis acidity of the sites in the specific reaction–solvent system. Due to the similar apparent activation energies in these zeolites, commensurate differences in activity were observed throughout the experimental temperature range (Fig. 2). However, for Ti-Beta, an apparent activation energy of 69.0 ± 2.2 kJ mol^{-1} was calculated, which translates to a rate constant that is three orders of magnitude smaller than that of Hf-Beta at 423 K.

The apparent activation energy consists of the sum of the activation energy of the hydride shift and the enthalpy of adsorption of ML onto a site already occupied by a bound BuOH molecule (Eq. (9)). Our results indicate that the E_a of the hydride shift and the adsorption enthalpy of ML are either very similar for Sn-, Zr-, and Hf-Beta or that the differences in E_a and adsorption enthalpies for each catalyst exactly offset to give the same apparent energies. We would expect Zr- and Hf-Beta to have similar E_a and adsorption values since Hf and Zr have a similar size and electronic structure (s–d valence orbitals). However, it is surprising that Sn-Beta features similar apparent activation energy values, since Sn has a significantly smaller atomic radius and s–p valence electron orbitals. Evidently, the barriers for the hydrogen shift depend on the electronics of the entire reaction site, not just the metal atom alone. The $E_{a,H}$ comprises numerous energetic contributions involving the heteroatom and its effect on the solvent, reactants and transition state, including the following: site geometry, charge transfer, and polarizability. In addition, it is unknown whether the adjacent hydroxyl group of the open site plays a role in transition state stabilization. Therefore, different energetic contributions could offset to give the same total apparent activation energy. Recently, Li et al. highlighted this balancing effect with an extended QM/MM model of heteroatom-containing zeolites for glucose–fructose isomerization [52]. It was reported that although the metal centers and the adjacent hydroxyl groups in Sn- and Zr-Beta have drastically different polarizabilities and Brønsted basicities, respectively, their contribution summed to almost the same apparent activation energy.

Pre-exponential factors for Hf-, Zr-, Sn-, and Ti-Beta are all within an order of magnitude, but they reflect the difference in relative reaction rates observed across the experimental temperature range (Table 2). Although the differences in the experimental pre-exponential factors are not statistically significant to 90% confidence (Table S2, Supporting Information), we expect to see differences in the free energy of binding and reaction depending on the identity of the heteroatom. Changes in site geometry or energetics likely restrict available conformations of bound intermediates and the transition state. In addition, varying binding strengths may contribute to differences in vibrational frequencies of bound species. These differences in free energy may stabilize the transition from reactants to the six-membered ring transition state for certain heteroatoms, leading to the observed differences in reaction rate.

The observed differences in initial rates that exist for catalysts possessing similar activation barriers could also be a result of different proportions of catalytically active sites with respect to total metal content. Previous studies of Ti- and Sn-Beta showed that the distribution of open sites was highly dependent on catalyst pretreatment such as calcination conditions, as well as initial

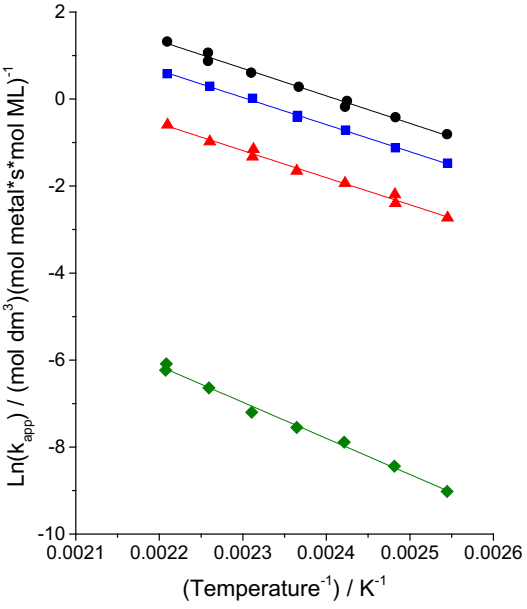

Fig. 2. Arrhenius plot for the MPV reduction of 0.02 mol dm^{-3} ML in 2-butanol solvent with various zeolite-beta catalysts. Hf-Beta (●), Zr-Beta (■), Sn-Beta (▲), Ti-Beta (◆). Rates are measured in moles of GVL produced per second normalized per total mole metal center in the catalyst. All liquid-phase flow reactions were performed under differential conditions in a packed-bed reactor pressurized under nitrogen at 20 bar with a flow rate range of 0.5–2.5 ml min^{-1}, with temperature range of 393–453 K.

exposure to the reaction environment [46,53]. The metal centers may interconvert between open and closed sites at reaction conditions. Different metal centers may have different M—O—Si hydrolysis rates, which would lead to different distributions of open and closed sites between the metals. At this time we cannot deconvolute these effects in our experimental data. The ability to quantitatively compare experimental kinetic parameters will facilitate the search for which fundamental physical properties are most important in predicting catalyst activity.

3.6. Comparison of hydrogen donor properties

We studied the effect of varying the position of the hydroxyl group and the carbon chain length of the hydrogen donor. Lewis acidity is highly dependent on the solvent environment, so it is important to study how solvent-catalyst systems may be optimized for higher activity [54,55]. The activation energies, pre-exponential factors, and rate constants at 423 K for the MPV reduction of ML over Hf-Beta are shown in Table 3. We found the most dramatic effect on the reaction rates was achieved by switching from a secondary to a primary alcohol donor (Fig. 3). BuOH, 2-propanol (2-PrOH), and cyclopentanol (Cy-PeOH) have activation energies of 52.5 ± 1.9, 46.3 ± 2.7, and 56.9 ± 2.2 kJ mol^{-1}, respectively, whereas 1-butanol (1-BuOH), 1-propanol (1-PrOH), and ethanol (EtOH) have activation energies of 73.5 ± 4.4, 69.2 ± 2.9, and 70.2 ± 4.2 kJ mol^{-1}, respectively. We hypothesize that the lower apparent activation barrier is primarily due to the stabilization of the hydride shift transition state by the electron-donating alpha terminal methyl group in secondary alcohols, which leads to a lower $E_{a,H}$. This can be quantitatively represented by the oxidation enthalpies of the respective alcohols, which clearly segregate between the primary and secondary alcohols (Table S3, Supporting Information). The pre-exponential factors for the reactions with primary alcohols are nearly two orders of magnitude greater than those for the secondary alcohols; a statistically significant result at 90% confidence (Table S2, Supporting Information). The absence of the alpha terminal methyl group likely reduces steric hindrance on both the bound intermediates and the transition state. Also, primary alcohols have access to a second C-1 hydrogen that can be transferred to ML during the six-membered ring transition state. This contributes both conformational and rotational degrees of freedom to the free energy along the reaction pathway. However, the larger pre-
exponential factors of primary alcohols do not compensate for their unfavorable activation energies at the temperatures investigated; the reaction rate constants for primary alcohols are an order of magnitude lower than their secondary counterparts at 423 K (Table 3). The higher rates for secondary alcohols have been previously reported for transfer hydrogenations using primary and secondary alcohols over supported ruthenium catalysts [56].

Longer alcohol chains increase reaction rates relative to shorter chains. This effect is observed primarily in the pre-exponential factors, as the activation energies are nearly the same within the primary and secondary alcohol groups. The pre-exponential factor of 2-PrOH is an order of magnitude lower than that of BuOH, and a similar decrease is seen when switching from 1-BuOH to 1-PrOH. In contrast, there is only a threefold decrease in pre-exponential factor when switching from 1-PrOH to EtOH. The polarity of the alcohol, quantitatively represented by its dielectric constant, increases with decreasing chain length for the non-cyclic alcohols (Table S3, Supplemental Information). Cy-PeOH has a dielectric constant that lies in-between that of BuOH and 2-PrOH, and we see the same trend in the pre-exponential factors. An increase in solvent polarity most likely results in tighter binding to the Lewis acid center, and therefore, a decrease in flexibility of the bound intermediate and transition state. The importance of binding flexibility is evident in the large decrease in apparent rate constant, from 1.33 to 0.196 (mol dm^3)(mol metal s mol ML)$^{-1}$, when using Cy-PeOH instead of BuOH. The rigid structure of cyclopentanol limits the number of accessible conformations leading to a higher penalty for binding. The differences in solvent polarity may also lead to different partitioning in the hydrophobic zeolite pores and affect the strength of solvation of ML [57–60]. We note that the sizes of all studied alcohols are smaller than the size of a Beta zeolite pore [30]. Therefore, this work captures the trends of solvents that should be largely unaffected by constriction due to the pore size. It is important to determine how catalyst activity is affected by small changes in substrate geometry in order to increase the flexibility of catalytic processes to adapt to varying feedstocks.

3.7. Kinetic model of packed-bed reactor

An ideal packed-bed reactor kinetic model was developed to quantitatively describe the reduction of ML in BuOH over an Hf-Beta catalyst. The reactor was assumed to operate under isothermal and constant pressure condition, with no radial gradients in concentration, temperature, or reaction rate. For the derivation, we used the simplified rate expression (Eq. (13)), which has first-order dependence on ML concentration (mol dm^{-3}) and the temperature dependent apparent rate constant k_{app} ((mol GVL dm^3)(mol metal s mol ML)$^{-1}$). This apparent rate constant can be calculated from the Arrhenius parameters (Eq. (14)) determined from initial rate experiments listed in Tables 2 and 3.

$$r' = k_{app} C_{ML} \quad (13)$$

Table 3
Measured first-order rate constants, activation energies and pre-exponential factors for MPV reduction of methyl levulinate (ML) in hydrogen-donating solvents (BuOH, 2-butanol; 1-BuOH, 1-butanol; 2-PrOH, 2-propanol; 1-PrOH, 1-propanol; EtOH, ethanol; Cy-PeOH, cyclopentanol) with Hf-Beta catalyst. Rates are measured in moles of GVL produced per second normalized per total mole metal center in the catalyst. All liquid-phase flow reactions were performed in a packed-bed reactor pressurized under nitrogen at 20 bar with a flow rate range of 0.5–2.5 ml/min, with temperature range of 393–453 K.

Run	Catalyst	Feed (mol dm^{-3})	Solvent	Rate constant k_{app} at 423 K[a]	Apparent E_a (kJ mol^{-1})	Standard error[b] (kJ mol^{-1})	Pre-exponential factor A[c]	Standard multiplicative error[b,c]
1	Hf-Beta	0.02 ML	BuOH	1.33E+0	52.5	1.9	41.3	1.7
6	Hf-Beta	0.02 ML	1-BuOH	1.64E−1	73.5	4.4	1508.7	3.5
7	Hf-Beta	0.02 ML	2-PrOH	7.35E−1	46.3	2.7	3.4	2.1
8	Hf-Beta	0.02 ML	1-PrOH	5.41E−2	69.2	2.9	189.6	2.3
9	Hf-Beta	0.02 ML	EtOH	1.44E−2	70.2	4.2	68.8	3.3
10	Hf-Beta	0.02 ML	Cy-PeOH	1.96E−1	56.9	2.2	20.6	1.9

[a] Units: (mol dm^3)(mol metal s mol ML)$^{-1}$.
[b] Standard error of regression assuming errors are normally distributed, sum of square residuals is χ^2 distributed with $n-2$ degrees of freedom.
[c] Units: 10^5 (mol dm^3)(mol metal s mol ML)$^{-1}$.

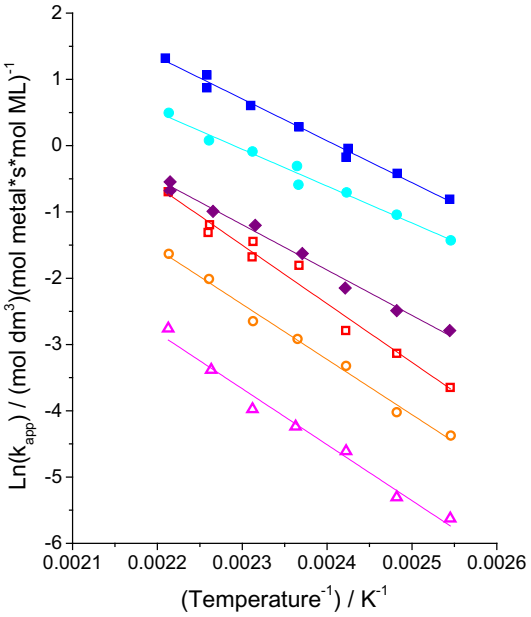

Fig. 3. Arrhenius plot for the MPV reduction of ML with Hf-Beta using different hydrogen donors (BuOH, 2-butanol; 1-BuOH, 1-butanol; 2-PrOH, 2-propanol; 1-PrOH, 1-propanol; EtOH, ethanol; Cy-PeOH, cyclopentanol). 0.02 mol dm^{-3} ML in 2-BuOH (■), 0.02 mol dm^{-3} ML in 1-BuOH (□), 0.02 mol dm^{-3} ML in 2-PrOH (●), 0.02 mol dm^{-3} ML in 1-PrOH (○), 0.02 mol dm^{-3} ML in EtOH (△), 0.02 mol dm^{-3} ML in Cy-PeOH (◆). Rates are measured in moles of GVL produced per second normalized per total mole metal center in the catalyst. All liquid-phase flow reactions were performed under differential conditions in a packed-bed reactor pressurized under nitrogen at 20 bar with a flow rate range of 0.5–2.5 ml min^{-1}, with temperature range of 393–453 K.

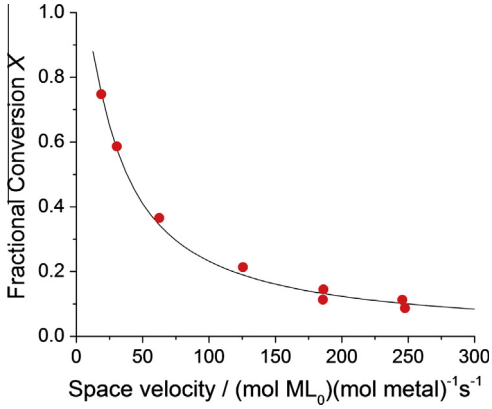

Fig. 4. Comparison between experimental and model-predicted conversion of ML to GVL using 2-butanol with Hf-Beta catalyst at various space velocities. Liquid-phase flow reactions were performed in a packed-bed reactor pressurized under nitrogen at 15 bar with a flow rate range of 0.3–5.0 ml min^{-1}, 0.02 mol dm^{-3} ML at 423 K.

$$k_{app} = A_{app} \exp\left(\frac{E_{a,app}}{RT}\right) \tag{14}$$

The concentration profile for a packed-bed-reactor is given in Eq. (15). The detailed derivation for this equation is shown in section C of the Supporting Information.

$$X = 1 - \exp\left(\frac{C_{ML,0} k_{app}}{SV}\right) \tag{15}$$

X is the conversion in terms of GVL production, SV is the space velocity (mol ML$_0$)(mol metal s)$^{-1}$, and $C_{ML,0}$ is the initial concentration of ML.

Fig. 4 shows the experimental values superimposed over the concentration profiles predicted by the model at space velocities in a range of 10–300 (mol ML$_0$)(mol metal s)$^{-1}$ and conversions ranging from 10% to 80%. There exists good agreement between the experimental and theoretical values obtained with the activation energies and pre-exponential factors calculated in previous sections. As such, we can model the behavior of the ML to GVL reaction using each of the different hydrogen-donating solvents as well as each of the different Beta catalysts with high fidelity.

4. Conclusions

Hf-Beta was determined to be a highly active and selective catalyst for the MPV reduction of ML to 4HP and subsequent ring closing to GVL in 2-butanol. The reaction was confirmed to be first order in ML in 2-butanol solvent, and first order in 2-butanol in ML solvent. This supports a dual-binding mechanism where the ketone and alcohol interact with a single metal site forming a six-membered transition state. The absence of intercrystalline and intracrystalline mass and heat transport limitations was confirmed by varying linear velocities and varying Beta zeolite metal content. A KIE value of ca. 2 corroborated that the rate-determining step is in fact the hydride shift, and that the transition state is dominated by bending rather than stretching vibrational modes. The apparent activation energy of the reaction over Hf-Beta was 52.5 kJ mol^{-1}, which is similar to activation energies for LA hydrogenation and computational studies. We found that Hf-Beta was the most active out of Ti-, Sn-, and Zr-Beta catalysts. Sn-, Zr-, and Hf-Beta all had very similar activation energies, while that of Ti-Beta was higher at 69.0 kJ mol^{-1}. A study of varying the hydrogen donor properties showed that secondary alcohols are much more active than primary alcohols with activation energies that are ca. 20 kJ mol^{-1} lower, most likely due to transition state stabilization of the C-1 position during the hydride shift. In addition, decreasing chain length of the alcohol did not have an effect on the activation energies but did decrease the pre-exponential factors leading to three- to ten-fold decreases in rates in the experimental temperature range. We developed a kinetic model using the experimentally determined activation energies and pre-exponential factors to accurately predict conversions in a packed-bed reactor.

This study provides the first quantification of kinetic parameters for the MPV reduction of liquid-phase substrates on zeolite Lewis acid catalysts. In addition, we provide a fully quantitative comparison of Ti-, Sn-, Zr-, and Hf-Beta initial rate constants, apparent activation energies, and pre-exponential factors for the reduction of ML in 2-butanol. Experimentally quantifying the effects of varying Lewis acid metal centers and substrates is crucial for the design of effective heterogeneous catalysts for applications in biomass conversion.

Acknowledgments

The authors acknowledge financial support for this work from the U.S. Department of Energy, Office of Science, Office of Basic Energy Sciences, Chemical Sciences, Geosciences and Biosciences Division under Grant No. DE-FG02-12ER16352. We also thank Marco B. Wonink and Anthony Crisci (Massachusetts Institute of Technology, Chemical Engineering) for their support in building the infrared spectroscopy *in situ* dosing system.

Appendix A. Abridged derivation of ML MPV turnover rate expression

Here, we show an abridged derivation of the rate expression for GVL production (Eq. (6)) from the MPV reduction of ML with 2-butanol (BuOH) as the hydrogen donor. The sequence of

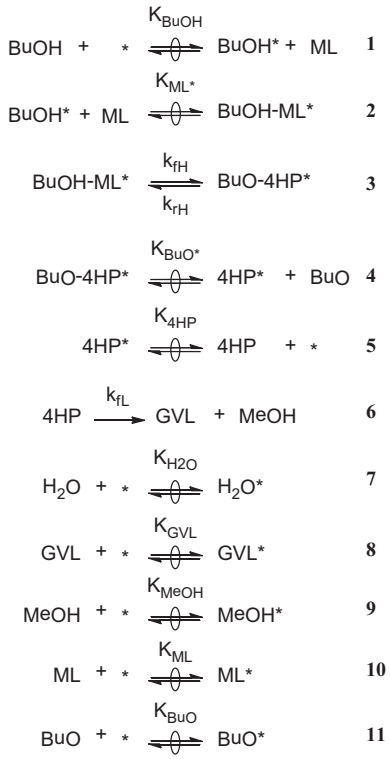

Scheme A2. Proposed elementary steps for the catalytic cycle of the MPV reduction of methyl levulinate (ML) to 4-hydroxypentanoate (4HP) with 2-butanol (BuOH) over a partially hydrolyzed metal site in zeolite framework (*). Singly-bound species can reversibly deactivate the catalytic site as shown in equations steps 7–11. Doubly-bound inhibitors are assumed to be negligible.

elementary steps is shown in Scheme A2. A complete derivation is given in section B in the Supporting Information. The kinetically-relevant step is the hydride shift (step 3) based on the observed H/D KIE of ~2 at 423 K on Hf-Beta when using 2-propanol-D_8 reactant (Section 3.3). All the adsorption and desorption steps are assumed to be quasi-equilibrated, including steps 7–11, which allow species to bind and inhibit active sites. These steps are depicted as single adsorption and desorption steps even though they may represent a combination of elementary steps, such as deprotonation to form alkoxides. We also assume that the intramolecular ring closing (step 6) is very fast and essentially irreversible. This assumption is reasonable given the reaction conditions at 423 K, the presence of Brønsted acidity in the zeolite catalyst, and no detectable 4HP when analyzing reaction solutions. The rate expression for the rate-determining step is (mol dm^{-3} s^{-1}):

$$r_{rds} = k_{f,H} C_{BuOH-ML^*} - k_{r,H} C_{BuO-4HP^*} \quad (A1)$$

where C_i are the concentration of species i (mol dm^{-3}), and k_i (s^{-1}) are the forward and reverse rate constants for the hydride shift. The quasi-equilibrium assumption gives us the following expressions in terms of the adsorption/desorption equilibrium constant $K = \frac{k_{ads}}{k_{des}}$ (dm^3 mol^{-1}) for each species. We show only the expression for steps 1 and 2.

$$K_{BuOH} = \frac{C_{BuOH^*}}{C_{BuOH} C_*} \quad (A2)$$

$$K_{ML^*} = \frac{C_{BuOH-ML^*}}{C_{BuOH^*} C_{ML}} \quad (A3)$$

We assume pseudo-steady-state on the concentration of 4HP intermediate, and that the rate constant for lactonization ($k_{f,L}$), is extremely large. After rearranging, we find the concentration of 4HP to be close to 0, which is supported by GC analysis of reaction solutions. This means the concentration of bound intermediate 4HP species is also close to 0. This allows us to simplify Eq. (A1) to only the forward reaction. Replacing bound intermediates with solution phase species using the equilibrium Eqs. (A2) and (A3), we obtain a rate expression in terms of free active sites.

$$r_{rds} = k_{f,H} K_{ML^*} K_{BuOH} C_{ML} C_{BuOH} C_* \quad (A4)$$

Combining the Lewis acid total site balance with the equilibrium constant expressions and rearranging allows us to isolate C_*.

$$C_{*tot} = C_*(1 + K_{ML}C_{ML} + K_{BuOH}C_{BuOH} + K_{GVL}C_{GVL} + K_{H_2O}C_{H_2O} + K_{4HP}C_{4HP} + K_{MeOH}C_{MeOH} + K_{BuO}C_{BuO}) \quad (A5)$$

Substituting the expression for C_* into (A4) gives us:

$$r_{rds} = \frac{k_{f,H} K_{ML^*} K_{BuOH} C_{ML} C_{BuOH} C_{tot^*}}{D}$$
$$D = 1 + K_{ML}C_{ML} + K_{BuOH}C_{BuOH} + K_{GVL}C_{GVL} + K_{H_2O}C_{H_2O} + K_{4HP}C_{4HP} + K_{MeOH}C_{MeOH} + K_{BuO}C_{BuO} \quad (A6)$$

If we normalize the rate by the concentration of total acid sites, which is assumed to be the metal content in the zeolite, we get the expression:

$$r' = \frac{k_{f,H} K_{ML^*} K_{BuOH} C_{ML} C_{BuOH}}{D}$$
$$D = 1 + K_{ML}C_{ML} + K_{BuOH}C_{BuOH} + K_{GVL}C_{GVL} + K_{H_2O}C_{H_2O} + K_{4HP}C_{4HP} + K_{MeOH}C_{MeOH} + K_{BuO}C_{BuO} \quad (A7)$$

This rate has units of (mol (mol metal)$^{-1}$ s^{-1}). Further simplifications of this rate expression when using a large excess of either BuOH or ML are given in Section 3.2 Eqs. (7)–(12).

Appendix B. Supplementary material

Supplementary data associated with this article can be found, in the online version, at http://dx.doi.org/10.1016/j.jcat.2014.10.010.

References

[1] M.J. Climent, A. Corma, S. Iborra, Green Chem. 16 (2014) 516.
[2] M. Dusselier, M. Mascal, B.F. Sels, Top chemical opportunities from carbohydrate biomass: a chemist's view of the biorefinery, in: Top. Curr. Chem., Springer, Berlin, Heidelberg, 2014, pp. 1–40.
[3] C. Aellig, F. Jenny, D. Scholz, P. Wolf, I. Giovinazzo, F. Kollhoff, I. Hermans, Catal. Sci. Technol. 4 (2014) 2326–2331.
[4] S. Van de Vyver, J. Geboers, P.A. Jacobs, B.F. Sels, ChemCatChem 3 (2011) 82–94.
[5] M.J. Climent, A. Corma, S. Iborra, M.J. Sabater, ACS Catal. 4 (2014) 870–891.
[6] V.L. Sushkevich, I.I. Ivanova, S. Tolborg, E. Taarning, J. Catal. 316 (2014) 121–129.
[7] J.D. Lewis, S. Van de Vyver, A.J. Crisci, W.R. Gunther, V.K. Michaelis, R.G. Griffin, Y. Román-Leshkov, ChemSusChem 7 (2014) 2255–2265.
[8] L. Bui, H. Luo, W.R. Gunther, Y. Roman-Leshkov, Angew. Chem. Int. Ed. Engl. 52 (2013) 8022–8025.
[9] M. Chia, J.A. Dumesic, Chem. Commun. (Camb.) 47 (2011) 12233–12235.
[10] R. Gounder, M.E. Davis, J. Catal. 308 (2013) 176–188.
[11] H.J. Cho, P. Dornath, W. Fan, ACS Catal. 4 (2014) 2029–2037.
[12] M. Moliner, Y. Roman-Leshkov, M.E. Davis, Proc. Natl. Acad. Sci. USA 107 (2010) 6164–6168.
[13] R. Gounder, M.E. Davis, ACS Catal. 3 (2013) 1469–1476.
[14] Y. Román-Leshkov, M. Moliner, J.A. Labinger, M.E. Davis, Angew. Chem. Int. Ed. 49 (2010) 8954–8957.
[15] W.R. Gunther, Y. Wang, Y. Ji, V.K. Michaelis, S.T. Hunt, R.G. Griffin, Y. Román-Leshkov, Nat. Commun. 3 (2012) 1109.
[16] W.R. Gunther, Q. Duong, Y. Román-Leshkov, J. Mol. Catal. A: Chem. 379 (2013) 294–302.
[17] P.P. Pescarmona, K.P. Janssen, C. Delaet, C. Stroobants, K. Houthoofd, A. Philippaerts, C. De Jonghe, J.S. Paul, P.A. Jacobs, B.F. Sels, Green Chem. 12 (2010) 1083–1089.

[18] E. Taarning, S. Saravanamurugan, M. Spangsberg Holm, J. Xiong, R.M. West, C.H. Christensen, ChemSusChem 2 (2009) 625–627.
[19] C.M. Lew, N. Rajabbeigi, M. Tsapatsis, Microporous Mesoporous Mater. 153 (2012) 55–58.
[20] R. Cohen, C.R. Graves, S.T. Nguyen, J.M. Martin, M.A. Ratner, J. Am. Chem. Soc. 126 (2004) 14796–14803.
[21] E.J. Campbell, H. Zhou, S.T. Nguyen, Org. Lett. 3 (2001) 2391–2393.
[22] D.A. Evans, S.G. Nelson, M.R. Gagne, A.R. Muci, J. Am. Chem. Soc. 115 (1993) 9800–9801.
[23] B.P. Warner, J.A. D'Alessio, A.N. Morgan III, C.J. Burns, A.R. Schake, J.G. Watkin, Inorg. Chim. Acta 309 (2000) 45–48.
[24] V. Ivanov, J. Bachelier, F. Audry, J. Lavalley, J. Mol. Catal. 91 (1994) 45–59.
[25] M.a.A. Aramendıa, V. Borau, C. Jiménez, J.M. Marinas, J.R. Ruiz, F.J. Urbano, Appl. Catal. A 244 (2003) 207–215.
[26] P.S. Kumbhar, J. Sanchez-Valente, J. Lopez, F. Figueras, Chem. Commun. (1998) 535–536.
[27] C. Jiménez-Sanchidrián, J.R. Ruiz, Appl. Catal. A 469 (2014) 367–372.
[28] E. Creyghton, S. Ganeshie, R. Downing, H. Van Bekkum, J. Mol. Catal. A: Chem. 115 (1997) 457–472.
[29] J.C. van der Waal, K. Tan, H. van Bekkum, Catal. Lett. 41 (1996) 63–67.
[30] A. Corma, M.E. Domine, S. Valencia, J. Catal. 215 (2003) 294–304.
[31] A. Corma, M.E. Domine, L. Nemeth, S. Valencia, J. Am. Chem. Soc. 124 (2002) 3194–3195.
[32] Y. Zhu, G. Chuah, S. Jaenicke, J. Catal. 227 (2004) 1–10.
[33] M. Moliner, Dalton Trans. 43 (2014) 4197–4208.
[34] M. Dusselier, P. Van Wouwe, S. De Smet, R. De Clercq, L. Verbelen, P. Van Puyvelde, F.E. Du Prez, B.F. Sels, ACS Catal. 3 (2013) 1786–1800.
[35] H.Y. Luo, L. Bui, W.R. Gunther, E. Min, Y. Román-Leshkov, ACS Catal. 2 (2012) 2695–2699.
[36] J.J. Pacheco, M.E. Davis, Proc. Natl. Acad. Sci. USA 111 (2014) 8363–8367.
[37] W.R. Gunther, V.K. Michaelis, M.A. Caporini, R.G. Griffin, Y. Román-Leshkov, J. Am. Chem. Soc. 136 (2014) 6219–6222.
[38] Y. Román-Leshkov, M.E. Davis, ACS Catal. 1 (2011) 1566–1580.
[39] I.T. Horváth, H. Mehdi, V. Fábos, L. Boda, L.T. Mika, Green Chem. 10 (2008) 238.
[40] J.Q. Bond, D.M. Alonso, D. Wang, R.M. West, J.A. Dumesic, Science 327 (2010) 1110–1114.
[41] L. Qi, I.T. Horváth, ACS Catal. 2 (2012) 2247–2249.
[42] D.M. Alonso, S.G. Wettstein, J.A. Dumesic, Green Chem. 15 (2013) 584.
[43] E.I. Gürbüz, D.M. Alonso, J.Q. Bond, J.A. Dumesic, ChemSusChem 4 (2011) 357–361.
[44] J.S. Luterbacher, J.M. Rand, D.M. Alonso, J. Han, J.T. Youngquist, C.T. Maravelias, B.F. Pfleger, J.A. Dumesic, Science 343 (2014) 277–280.
[45] R.S. Assary, L.A. Curtiss, J.A. Dumesic, ACS Catal. 3 (2013) 2694–2704.
[46] M. Boronat, A. Corma, M. Renz, J. Phys. Chem. B 110 (2006) 21168–21174.
[47] A. Corma, L.T. Nemeth, M. Renz, S. Valencia, Nature 412 (2001) 423–425.
[48] M. Boronat, P. Concepción, A. Corma, M. Renz, S. Valencia, J. Catal. 234 (2005) 111–118.
[49] S. Roy, K. Bakhmutsky, E. Mahmoud, R.F. Lobo, R.J. Gorte, ACS Catal. 3 (2013) 573–580.
[50] O.A. Abdelrahman, A. Heyden, J.Q. Bond, ACS Catal. 4 (2014) 1171–1181.
[51] P. Nandi, Y.I. Matvieiev, V.I. Boyko, K.A. Durkin, V.I. Kalchenko, A. Katz, J. Catal. 284 (2011) 42–49.
[52] Y.-P. Li, M. Head-Gordon, A.T. Bell, ACS Catal. 4 (2014) 1537–1545.
[53] R. Bermejo-Deval, R.S. Assary, E. Nikolla, M. Moliner, Y. Román-Leshkov, S.-J. Hwang, A. Palsdottir, D. Silverman, R.F. Lobo, L.A. Curtiss, Proc. Natl. Acad. Sci. USA 109 (2012) 9727–9732.
[54] C. Laurence, J.-F. Gal, Lewis Basicity and Affinity Scales: Data and Measurement, John Wiley & Sons, 2009.
[55] C. Laurence, J. Graton, J.-F. Gal, J. Chem. Educ. 88 (2011) 1651–1657.
[56] P. Panagiotopoulou, N. Martin, D.G. Vlachos, J. Mol. Catal. A: Chem. 392 (2014) 223–228.
[57] J. Stelzer, M. Paulus, M. Hunger, J. Weitkamp, Microporous Mesoporous Mater. 22 (1998) 1–8.
[58] E.E. Mallon, I.J. Babineau, J.I. Kranz, Y. Guefrachi, J.I. Siepmann, A. Bhan, M. Tsapatsis, J. Phys. Chem. B 115 (2011) 11431–11438.
[59] R. Gounder, M.E. Davis, AlChE J. 59 (2013) 3349–3358.
[60] R. Gounder, Catal. Sci. Technol. 4 (2014) 2877–2886.